Electrical Architecture of 90-seater Electric Aircraft

A Cable Perspective

Guo, Ruochen; Dong, Jianning; Wolleswinkel, Rob E.; De Vries, Reynard; Niasar, Mohamad Ghaffarian

DOI
10.1109/TTE.2024.3517838

Publication date
2024

Document Version
Final published version

Published in
IEEE Transactions on Transportation Electrification

Electrical Architecture of 90-Seater Electric Aircraft: A Cable Perspective

Ruochen Guo, *Member, IEEE*, Jianning Dong, *Senior Member, IEEE*, Rob E. Wolleswinkel, Reynard de Vries, and Mohamad Ghaffarian Niasar, *Member, IEEE*

***Abstract*— Optimized power system architectures and lighter weight are enabling considerations for the successful development of all-electric aircraft (AEA). In this article, a cross-redundant connection architecture and weight reduction solutions are investigated for a 90-seater full battery-electric aircraft from the perspective of high-power aviation cable. Design criteria of the power system architecture are introduced. Material selection, sizing, and weight estimation methods of cable for AEA are discussed by combining ground cable standards with aviation requirements. The influence of the conductor materials, voltage level, current, battery pack quantity, and operating temperature on cable evaluation is thoroughly discussed and analyzed. Weight comparison under two controversial voltage level options (800 V and 3 kV) is conducted. Comparison results show that the use of an aluminum conductor, polytetrafluoroethylene (PTFE) insulator, and a voltage level of 3 kV proves to be a preferable selection for current AEA medium and high voltage cables. Increasing the rating operation temperature to 120 °C is a conservative and secure option. The layout of battery packs consistent with the quantity of distributed electric motors is preferable to achieve the lightest cabling system. This study provides a guideline for the cable sizing methods of high-power aviation cables and an optimized design solution for the power system architecture of AEA from the perspective of cable layout and weight assessment.**

***Index Terms*— All-electric aircraft (AEA), aviation cable, cable weight estimation, direct current power architecture, electric power system.**

I. Introduction

CARBON neutrality and the reduction of carbon emissions are critical topics that humanity needs to address both in the present and the future [1]. Sustainable development goals have been introduced to tackle global challenges and combat climate change [2], [3], [4]. Statistics show that aviation globally is responsible for more than 2.4% of all greenhouse gas emissions [5]. Environmental concerns in transportation give rise to the development of electrification in the aerospace field. In addition, aircraft operation costs are expected to increase in the long term, which will result in a lower profit margin as the fuel price is increasing. These factors prompt airlines and aircraft manufacturers to actively seek new solutions and adopt innovative flight concepts and technologies to achieve environmentally friendly and cost-effective flying [3]. The electrification of aircraft is an inevitable future development trend for tackling these challenges. Over the past decades, the concept of more electric aircraft (MEA) and all-electric aircraft (AEA) has, therefore, attracted significant attention, and many attempts have been made [6], [7], [8], [9]. MEA, such as Airbus 380 and Boeing 787, have been commercialized, which lays the first step toward the achievable electrification of aircraft [6], [7]. The electrification rates of both aircraft are, however, actually low, not exceeding 2%. To evaluate the electrification rate, P_{el}/P_{th} can be considered where P_{el} is the consumed electrical power and P_{th} is the maximum required thrust power during takeoff. Some hybrid electric aircraft projects, such as E-FAN X, NASA STARC-ABL, and N3-X, are also dedicated to advancing the electrification rates of aircraft [8]. Given the current and expected battery technology, in most literature, battery-electric aircraft are only considered feasible for short ranges (<400 km) and small payloads (<19 pax). As a result, battery-electric aircraft development focuses on new aviation segments such as regional and urban air mobility [10]. An 80–150 passenger narrow body, single-aisle AEA that properly operates over typical commercial missions is still a long-term target [9]. In 2024, scholars from Elysian Aircraft and Delft University of Technology reexamined that full battery-electric powered 90-seater aircraft would be feasible based ON current battery technology with only a minor structural optimization of existing larger aircraft [10], [11]. This provides theoretical feasibility for the electrification of large aircraft. The electrical architecture design, however, has not been elaborated.

AEA means that all the thrust components will be replaced by electrical systems; therefore, a reasonable electric power system architecture provides a solution for aircraft electrification. The power system of AEA is an onboard microgrid, and a dc power transmission system is preferable. The ground power system concept provides inspiration for the design of electric architectures on aircraft [12]. Direct connection, cross-redundant connection, and ring network are common concepts

Received 3 August 2024; revised 3 November 2024; accepted 9 December 2024. Date of publication 18 December 2024; date of current version 26 March 2025. *(Corresponding author: Mohamad Ghaffarian Niasar.)*

Ruochen Guo was with High Voltage Technology Group, Department of Electrical Sustainable Energy, Delft University of Technology, 2628 CD Delft, The Netherlands. He is now with Hitachi Energy Research, 72226 Västerås, Sweden (e-mail: ruochen.guo@hitachienergy.com).

Jianning Dong is with the DC Systems, Energy Conversion and Storage Group, Department of Electrical Sustainable Energy, Delft University of Technology, 2628 CD Delft, The Netherlands (e-mail: J.Dong-4@tudelft.nl).

Rob E. Wolleswinkel and Reynard de Vries are with Elysian Aircraft, 3641SK Mijdrecht, The Netherlands (e-mail: rob@elysianaircraft.com; reynard@elysianaircraft.com).

Mohamad Ghaffarian Niasar is with the High Voltage Technology Group, Department of Electrical Sustainable Energy, Delft University of Technology, 2628 CD Delft, The Netherlands (e-mail: M.GhaffarianNiasar@tudelft.nl).

Digital Object Identifier 10.1109/TTE.2024.3517838

used in electric architectures of AEA [13], [14]. Tailor-made optimization based on aircraft geomertry and location of different components is necessary. Because of the complex aircraft structures, diverse electrical components, and tens of megawatt level propulsive power, the design of the power system architecture is a trade-off process. AEA prioritizes high reliability and reduced weight as key criteria [5], [13]. The power transmissions and components are sized considering safe flight and single-point failure requirements [13], [14]. An accurate definition of reliability criteria and a deeper understanding of components weight optimization are, therefore, beneficial to achieve a successful onboard power system. The application of design criteria for the large AEA is, however, lacking.

Unlike small aircraft, large electric aircraft have a large total power load (>10 MW), which means that the operating current in the power system is significantly higher. This greatly increases the weight of the internal connecting cables. In addition, due to the aircraft's large size, the total length of the cables spans several hundred meters, resulting in a larger weight ratio of cables among all onboard components [14]. Increasing the voltage level of the power system provides a viable method to decrease the weight of AEA. It is widely acknowledged that elevating state-of-the-art several hundred volts to 3 kV or even higher is an inevitable step in the aircraft electrification process [2], [5], [16]. Because of Paschen's law and low-pressure constraints, the highest voltage levels in the aviation industry are, however, usually below 1 kV. Although there are some standards and regulations related to aviation cables, there is still a lag in development of standards for high voltage aviation cabling system. Current standards are mainly focused on cables carrying hundreds of volts or on communication cables [17], [18]. Some of the requirements on cable design in these regulations do not fully address the development of future AEA and do not provide detailed guidance on specific sizing methods for selecting AEA cables. Investigating the design standard of high-power aviation cables is necessary for the development of green aviation. Integrating the design standards of ground cables with the existing aviation cable requirements allows for a feasible approach, but tailor-made cable assessment and further analysis are still needed [19], [20]. The effects of factors such as materials, voltage, current, operating temperature, etc., on AEA cables are not sufficiently clear.

Optimized cable evaluation methods should consider the effect on the whole system design as well. At the moment, the significant difference is the interconnections between various components, and that mainly affects the cable system weight. The effect of various quantities of power components (e.g., battery packs) and their layout on the cabling system weight is unclear. This lack of understanding would also limit a reasonable architectural design. In addition, comparing the differences in cable weight at different voltage levels (the current potential voltage level of 800 V and the future possible voltage level of 3 kV) can also clearly guide the aircraft weight budget.

In this work, a power system architecture is proposed based on 90-seater AEA, and a series of weight evaluations of high voltage high power cabling system are studied. This article is organized as follows. In Section II, an overview of the investigated aircraft and a cross-redundant connection architecture are introduced. In Section III, the material considerations, sizing methods, and weight estimation methods of the AEA cables are introduced in detail. In Section IV, the effect of the voltage variation, the number of battery packs, and the operating temperature are discussed, including the appropriate recommendations for cable sizing. The concept of power-sharing transmission is assessed from the perspective of cable weight. In Section V, six flight scenarios are discussed, the possible maximum current of different parts of cables is analyzed and the dominant scenario for the cable sizing is presented. Ultimately, Section VI compares the total weight of the cabling systems of two system voltage levels (800 V and 3 kV), offering a comprehensive assessment of their weight difference.

II. AEA Overview and Power System Architecture

A. Electric Aircraft Overview

E9X AEA is designed as a battery-electric 90-seater aircraft and the main power demand comes from the propulsion system with a continuous motor output 12 MW at the propeller shafts. In the target aircraft, power generation is designed to be provided by a distributed propulsion system, including eight electric motors. The motor power demands are sized by the power required at takeoff. The basic design of the electric power system is shown in Fig. 1.

The geometrical design of the E9X Aircraft is similar to that of the conventional one, but the internal electrical system and propulsion system are completely different and have been redesigned [9], [10]. The power system is a micro dc electrical system and includes a battery storage system, wiring harness, safety switches, dc–dc converters, electrical motors, thermal management system (TMS), mission range extenders, and other electrical loads. For normal flights, power is sourced exclusively from the battery packs distributed in the aircraft wings. The wiring harness plays a crucial role in connecting various components to ensure steady power transmission. Safety switches, such as circuit breakers (CBs) and high-voltage fuses, are installed to ensure the necessary protection in the event of component failures or short circuits. dc–dc converters close to the battery side boost the voltage level to high voltage dc busbar and the converters close to the TMS side convert the voltage to 270 V. The motors are strategically distributed in the wings to achieve a balanced configuration and ensure reasonable propulsion distribution. Each motor is rated at the same power level. TMS is responsible for cooling different electric components and producing the necessary thermal energy during the mission. In the event of a fully depleted battery or emergency, the reserve energy system (range extenders) kicks in to provide backup, ensuring a secure energy supply. The range extenders consist of a fuel tank, gas turbine, and generator, all connected to the dc power busbar.

The biggest difference between traditional aircraft and electric aircraft is that the megawatt, kilovolt level dc micro electric architecture needs to be redesigned to achieve a lighter

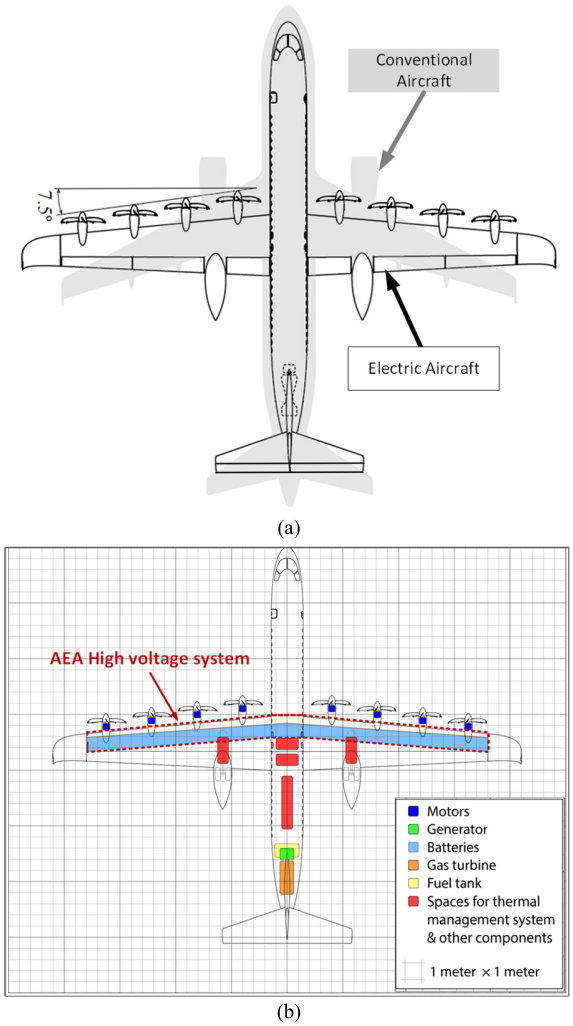

Fig. 1. Design schematic of AEA. (a) External structure of E9X (solid line). (b) Internal structure of E9X.

weight and different components need to be selected to meet the requirement of smooth flight and reliable operation [21]. The electric architectural design primarily revolves around key electrical components, including batteries, power electronics, switches, wirings, and motors. The range extender serves as an auxiliary system with limited involvement in the power supply. Even when in operation, the range extender relies on the dc system for energy transmission. The power architecture, therefore, only takes into account the power transmission lines connected to the range extender, excluding the extender itself from the scope of electrical design. TMS is also not directly engaged in power sources and propulsion and is, hence, out of scope.

B. Proposed Architecture

High reliability and reduced weight are criteria for the electric architecture design of AEA. Tailor-made optimization based on aircraft size and location of different components is necessary. Power transmissions and components are sized with the considerations for safe flight and $n - 1$ contingencies [13], [14]. The cross-redundant connection achieves higher reliability due to its capability to facilitate multifeeders and multisources, as depicted in Fig. 2. In the proposed architecture, the CB and fuse are connected in series near the battery side to provide reliable protection. In case of a CB failure or slow response, the fuse serves as a backup protective device to cut off the short current. dc–dc converter boosts the voltage and then connects to the sub-busbar. On the motor side, the inverter connects to the sub-busbar as well. The four central busbars are the hubs for power distribution.

The solid-colored lines represent a primary feed to the propulsor motors, and the colored dotted lines represent a secondary feed from a separate bus. In the event of either a battery pack failure or a bus failure, the affected motors can be fed from their secondary bus. If one motor fails, the corresponding main power supply battery will not be trapped. The proposed architecture can maintain high reliability of the aircraft's electrical power system. When a single failure occurs in the busbar, motor, or battery, the aircraft can still ensure reliable operation, which meets the reliability requirements of the aircraft mission. It applies not only to the mission range but also to the reserve distance. When the battery is exhausted and the range extender starts, energy can still be distributed to the motor by two busbar cables.

In practice, electric motors and battery packs are installed on both wings of the aircraft. Consequently, all electrical systems must be designed in accordance with the main power loads and sources. The primary electrical devices and wirings are predominantly distributed horizontally across the two wings. This configuration poses challenges in achieving simplified cabling, shorter cable lengths, and efficient energy supply. It can be observed that precise assessment of the cabling system's weight would be an important topic for aircraft design.

Table I shows the comparison between proposed architectures and other system architecture concepts [13], [14]. The cross-redundant design excels in reliability and fault tolerance due to its multifeeder and multisource setup, providing a high level of resilience and safety. Although it has moderate complexity and weight, its maintenance needs are manageable, and it meets stringent safety and redundancy requirements essential for aviation.

In contrast, the direct connection is simple and lightweight but lacks adequate reliability and fault tolerance, making it unsuitable for critical applications. The ring connection offers moderate reliability with rerouting capabilities but is heavier and more complex without fully compensating for these trade-offs in terms of reliability or suitability. Overall, the cross-redundant architecture best balances reliability, fault tolerance, and operational safety, making it the most viable choice for electric aircraft systems.

III. Aviation Cable Sizing Method

A. Cable Conductor Material Considerations

The conductor and insulator are critical parts for the cable sizing. There are two typical materials used when it comes to conductors in cables: copper and aluminum. Table II compares the material properties of copper and aluminum [22].

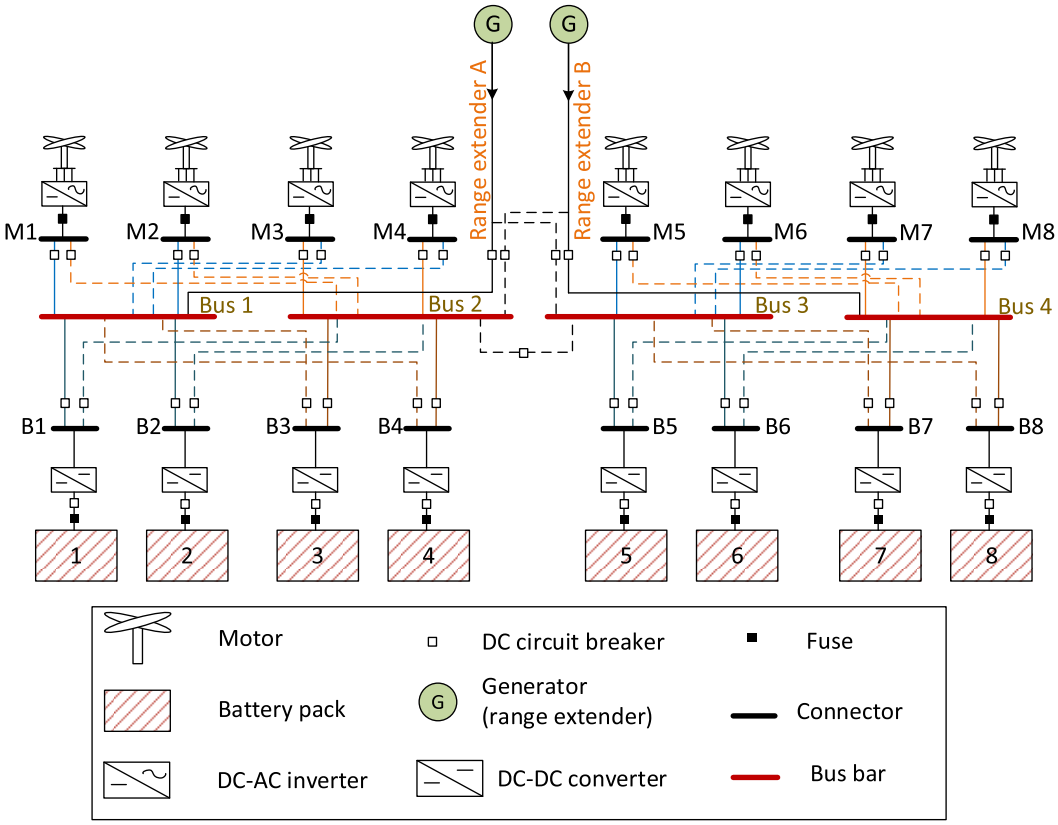

Fig. 2. Proposed Architecture for the power system of AEA (cross-redundant connection).

TABLE I
COMPARISON BETWEEN DIFFERENT ELECTRICAL SYSTEM ARCHITECTURES

Criteria	Proposed architecture	Direct connection [13-14]	Ring connection [13]
Reliability	**High** Multi-feeder, multi-source configuration	**High** Allows re-routing power supply	**Low** Single point of failure if one path fails
Fault Tolerance	**High**	**High**	**Low**
Complexity	**Moderate** Multiple connections and control logic	**High** Complex connections within the loop	**Low** Cimple direct paths
Weight	**Moderate** Additional cables and components add weight	**High** Additional cables and extra circuit breakers add weight	**Low** Minimal components and simple cabling syetem
Maintenance	**Moderate** Complex, but redundancy improves reliability during maintenance	**Moderate** Loop complexity can increase maintenance needs	**Easy** Minimal components simplify maintenance
Suitability	**High** Meets reliability and redundancy requirements for safety	**Moderate** Suitable but lacks full benefits in weight vs. reliability	**Low** Unsuitable due to poor reliability and limited fault tolerance

Copper has better electrical and thermal properties, such as higher conductivity, less heat production, smaller voltage loss, and higher melting point. Copper also has better mechanical properties and fatigue properties. A limitation for aerospace applications is that copper is heavier and might, however, lead to a heavy mass of cable.

B. Cable Conductor Sizing

The sizing of the cable conductor is mainly driven by the maximum current through the cable, and the temperature caused by cable resistance should also be considered in the cable conductor sizing.

The resistance per unit length of the cable conductor is expressed as

$$\frac{R}{l} = \frac{1}{\sigma S} \tag{1}$$

where R is the conductor resistance (Ω), l is the cable length (m), σ is the conductor conductivity ($\mathrm{s{\cdot}m^{-1}}$), and S is the cross-sectional area of the conductor ($\mathrm{m^2}$).

The actual resistance of conductor (R_{cable}) is affected by the operating temperature, and their relationship is described

as [22] and [23]

$$R_{\text{cable}} = R_{\text{ref}} \cdot (1 + \alpha_r (T_c - T_{\text{ref}})) \tag{2}$$

where T_c is the actual conductor temperature (°C) defined as the maximum high-temperature tolerance of the operating condition. α_r is the resistance-temperature scale factor ($°C^{-1}$) which defines the resistance change with a one-degree increase, and the value for different materials can be found in Table I. R_{ref} is the reference resistance at a given temperature T_{ref}, the equation of R_{ref} is

$$R_{\text{ref}} = \rho \cdot l / S = \rho \cdot l / \left(\pi r_c^2\right) \tag{3}$$

where ρ is the resistivity (Ω·m) of the conductor at the reference temperature, r_c is the conductor radius (m), commonly a length of 1 m is used for calculating unit loss.

The steady-state temperature of cable is reached when the heat equilibrium is achieved. In this case, the heat source is the loss generated in the conductor due to current. The heat is conducted away through the insulator and other layers of the cable and is dissipated to the environment. Heat convection and thermal radiation are two main ways of heat dissipation; therefore, the steady-state heat in the conductor is a function of the heat generated in the conductor, the heat radiated from the insulator and the convection heat from the insulator. The processes are described by the following equations [28]:

$$Q_c = I^2 R_{\text{cable}} \tag{4}$$

$$Q_{\text{convection}} = hA(T_i - T_{\text{amb}}) \tag{5}$$

$$Q_{\text{rad}} = \epsilon \sigma A \left(T_i^4 - T_{\text{amb}}^4\right). \tag{6}$$

The steady-state temperature can be obtained when the heat produced equals the heat dissipation, as shown below

$$Q_c = Q_{\text{convection}} + Q_{\text{rad}}. \tag{7}$$

Q_c is the heat (W) generated by the current in the conductor, I is the current (A) going through the cable, $Q_{\text{convection}}$ is the heat loss (W) due to convection, A is the outer area exposed (m^2), T_i is the insulator surface temperature, and T_{amb} is the ambient temperature. Here, T_{amb} is given by 40 °C, which is the highest ambient temperature the aircraft may tolerate while at the departure location, such as Dubai. Q_{rad} is the heat loss due to radiation. ϵ is the emissivity coefficient of the insulator, and 0.8 is assumed because the surrounding insulator is considered to be a gray body. σ is the Stefan-Boltzmann's constant and has a value of 5.67×10^{-8} W × m^{-2} × C^{-4} [24], [25]. h is the convection thermal coefficient, which is derived from the Nusselt relation [24], [25]

$$\text{Nu} = \frac{hl}{\lambda} = 0.36(\text{Gr} \cdot \text{Pr})^{1/4} \tag{8}$$

where Gr is the Grashof number defined as (9), and Pr is the Prandtl number with a value of 0.71 for air [26]

$$\text{Gr} = \frac{gl^3 \beta \Delta T}{v^2} \tag{9}$$

where g is the gravity constant, and β is the gas expansion coefficient, which for an ideal gas can be seen as the inverse of the average temperature [27]. Convection thermal coefficient h can be solved by (8) and (9), then T_i can be solved by (4)–(7).

TABLE II
MATERIAL PROPERTIES OF TWO CONDUCTOR MATERIALS

Conductor material	Copper	Aluminium
Conductor conductivity ($s \cdot m^{-1}$)	$5.87*10^7$	$3.69*10^7$
Material density ($kg \cdot m^{-1}$)	8900	2700
Thermal Conductivity ($W \cdot m^{-1} K^{-1}$)	400	237
Tensile Strength (MPa)	210	90
Modulus of Elasticity(GPa)	110	68
Fatigue property	No. of cycle: $300*10^6$	No. of cycle: $50*10^6$
Resistance-temperature scale factor($°C^{-1}$)	0.00394	0.00429

The conductor temperature is described as [25]

$$T_c = \frac{Q_c}{2\pi k_i} \ln\left(\frac{t_i + r_c}{r_c}\right) + \frac{Q_c}{2\pi k_j} n\left(\frac{t_i + r_c + t_s + t_j}{r_c + t_i + t_s}\right) + T_i \tag{10}$$

where k_i and k_j are the thermal conductivity's of the insulator and jacket layer (shown in Table II), t_s and t_j are the thickness of sheliding layer and jacket layer respectively.

Through a series of calculations, the relationship between the conductor radius and conductor temperature under a given voltage and current can be obtained. Then, the rating of conductor radius is decided by the expected safe operating temperature. In this work, the maximum temperature for the conductor sizing is set to be 120 °C. More detailed discussion is given in Section IV.

It is noted that the skin effect of cable is not considered. For dc cables, the skin effect is generally negligible. This is because the skin effect arises from the tendency of ac to concentrate near the surface of a conductor at higher frequencies due to constantly changing electromagnetic fields. In dc systems, however, the current flow is constant, with no oscillation, so the entire cross-sectional area of the conductor is used to carry the current uniformly.

The potential difference is determined by the cable conductor resistance and the current going through the conductor, and the voltage drop V_{drop} is expressed as

$$V_{\text{drop}} = R_{\text{cable}} \cdot I. \tag{11}$$

After selecting the conductor size, it is necessary to ensure that the voltage drop at the operating temperature of the cable with a given length meet the design requirement. Equation (11) can be also used for assessing the losses of the whole electrical system.

C. Cable Insulator Sizing

For AEA cables, there are challenges with arcing and arc tracking, partial discharge (PD), and thermal management that will be exacerbated at higher voltages and currents [16]. Different from the cables used in ground medium voltage direct current (MVdc) grids and submarines, aviation cable faces a wider range of temperatures. The minimum high-temperature tolerance should be 150 °C, and the lowest allowed temperature should reach −65 °C [17]. The cable should also be resistant to arcing and prevent PD during high altitude flights

TABLE III
MATERIAL PROPERTIES OF INSULATOR MATERIALS

Material properties		Insulator materials			
		PFTE	PFA	PI	XLPE
Electrical properties	Permittivity	2.1	2.1	3.5	2.3
	Dielectric strength (kV/mm)	60~80	70~80	60~80	35~50
	Material density (kg/m^3)	2170	2150	1380	930
Thermal properties	Thermal conductivity ($W*m^{-1}*K^{-1}$)	0.25	0.19	0.4	0.29
	Melting point (°C)	327	305	380	130
	Temperature range (°C)	-90~+260	-90~+260	-240~+260	-40~+90
Mechanical properties	Modulus of elasticity (GPa)	0.49	0.55	3.1	0.6
	Tensile strength (MPa)	24	28	96	18

because the air pressure decreases, and thereby, the breakdown voltage of air decreases at higher altitudes.

Table III compares the properties of different insulation materials used as cable insulators [28], [29], [30]. For cross-linked polyethylene (XLPE) cables on the ground, the allowable operating temperature used for cable sizing is 90 °C [21]. This means that XLPE cable is not suitable for aerospace applications, and a new selection of insulator materials should be made. It was also demonstrated that some high-temperature engineering polymer materials, such as polytetrafluoroethylene (PTFE), perfluoro alkoxy (PFA), and polyimide (PI), may be enhanced to withstand arc tracking and also have good thermal properties. They provide options for the AEA cable insulator. PTFE is the referenceable material commonly specified in aerospace [28]. Previous applications were applied at lower voltages, and the performance at high voltages, however, needs to be verified in practice. PI is commonly used in aviation control systems for small currents and low voltages. Compared to PTFE, the basic electrical and thermal properties of PFA are similar. PFA is more flexible but has a lower flex-life; it is not capable of enduring repetitive folding; therefore, PTFE is the best choice for the AEA high voltage cabling system.

The method used for calculating the thickness of insulation is known as the single-void discharge (SVD) method described in [31]. The method is not dependent on the conductor material, which allows for an analysis of copper and aluminum conductors in one equation. The insulation thickness is highly dependent on the maximum voltage that is applied over the cable, and the equation is

$$t_i = r_c \cdot \left(\exp\left(\frac{K \cdot V \cdot t_v}{\alpha \cdot r_c} \right) - 1 \right) + C. \tag{12}$$

t_v is the thickness of the void or inclusion, which is assumed to be 50 μm [31], [32] and α is the minimum breakdown voltage of air in the cavity, which is assumed to be 250 V [33], [34]. K is the shape factor of the void which is assumed to be spherical, and the equation can be expressed as

$$K = \frac{3\varepsilon}{1 + 2\varepsilon} \tag{13}$$

where ε is the permittivity of the insulator.

D. Cable Weight Estimation

There are several main parts contributing to the cable weight: conductor, insulator, shielding layer, and jacket. The method for estimating the mass of the cable is done by using the density of the materials within the cables. The mass of the conductor is calculated by the conductor material ρ_c, selected conductor cross-sectional area A_c, and the cable length l. The formula for this calculation is as follows:

$$m_c = \rho_c \cdot A_c \cdot l = \rho_c \cdot \pi r_c^2 \cdot l. \tag{14}$$

The insulator mass is described as

$$m_i = \rho_i \cdot A_i \cdot l = \rho_i \cdot \pi \cdot \left((r_c + t_i)^2 - r_c^2 \right) \cdot l. \tag{15}$$

Similarly, The shielding layer is the outer layer and serves as electromagnetic compatibility protection. The shielding area is determined by assuming a shielding thickness, t_s, which is 0.12 mm for the MVdc cable [17]

$$\begin{aligned} m_s &= \rho_s \cdot A_s \cdot l \\ &= \rho_s \cdot \pi \cdot \left((r_c + t_i + t_s)^2 - (r_c + t_i)^2 \right) \cdot l. \end{aligned} \tag{16}$$

The cable jacket is the outermost layer of a cable and serves to protect the internal components from physical damage, moisture, and other environmental factors. The thickness of the jacket is related to the diameter of cable D, which can be expressed as [19]

$$t_j = 0.035D + 1.0. \tag{17}$$

The total weight of the cable is the summation of conductor mass and insulator mass, shielding layer weight, and jacket weight; thus,

$$m_{\text{total}} = m_c + m_i + m_s + m_j. \tag{18}$$

IV. ANALYSIS OF INFLUENCING FACTORS ON CABLE SIZING

A. Conductor Materials Comparison and Voltage Influence

Once the power architecture is determined, both the power loads and supplied sources typically stabilize. The selection of voltage is one of the key factors influencing the trade-off in choosing power components for electric aircraft. Fig. 3 illustrates cable parameters under various voltage levels. In our calculations, the power level is set at 1.5 MW, and the cable length is 10 m. The chosen voltage range for comparison spans from 800 V to 3 kV.

As depicted in Fig. 3(a), an increase in voltage corresponds to a parabolic decrease in conductor radius, a phenomenon applicable to both copper and aluminum cables. Notably, the conductor radius of aluminum cables surpasses that of copper cables under the same conditions. This difference gradually diminishes as the voltage level rises. The conductor radius of copper cables is 85.5% of that for aluminum cables

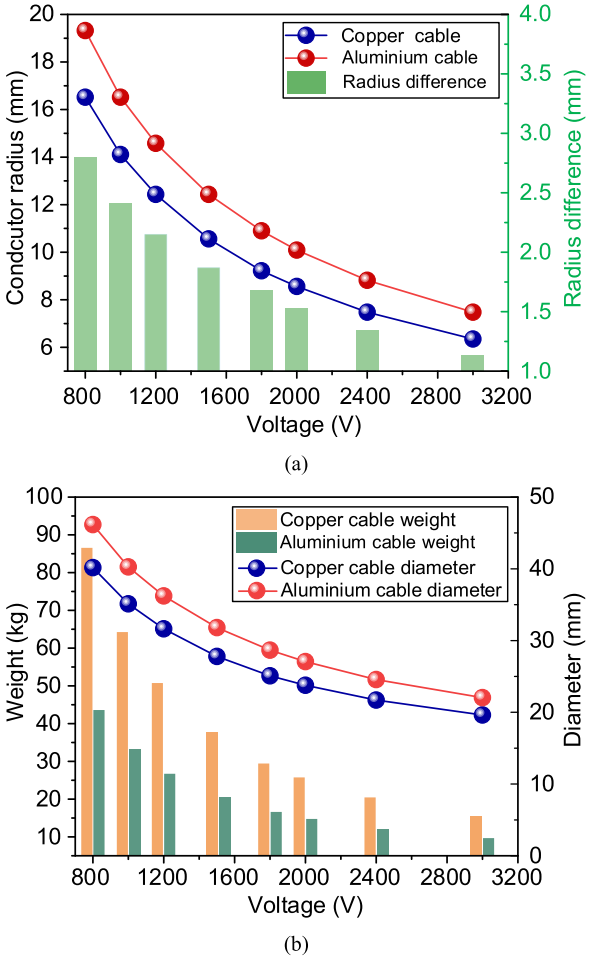

Fig. 3. Cable parameters under various voltages. (a) Cable conductor radius. (b) Cable weight and dimension.

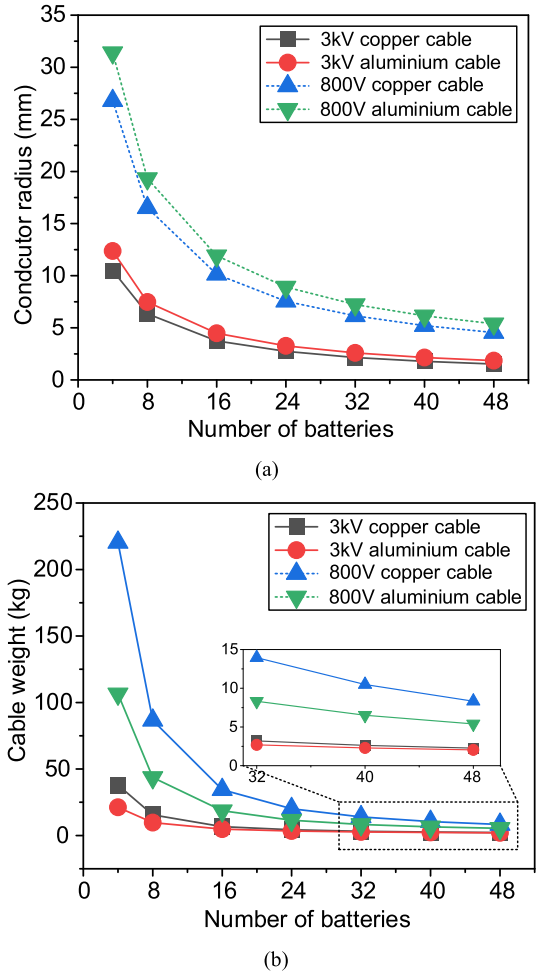

Fig. 4. Influence of the quantity of battery packs on the parameters of the connecting cables. (a) Relationship with the conductor radius. (b) Relationship with the cable weight (length: 10 m).

under 800 V. This ratio further reduces to 84.9% when the voltage is increased to 3 kV.

In Fig. 3(b), the variations in weight and cable diameter are presented. In spite of the aluminum cable having a larger conductor radius, its overall weight is lighter. At 800 V, the total weight of copper cable is 86.5 kg, while the aluminum cable weighs 43.6 kg. With an increase in voltage to 3 kV, the weight of the copper cable decreases to 15.6 kg, and the aluminum cable weight drops to 9.69 kg. The advantages of increasing voltage are particularly noticeable in weight reduction, especially for copper cables. As the voltage increases, the difference in diameter between two cables with different conductors decreases. At 3 kV, the cable diameter of the aluminum cable is only 2.5 mm greater than that of the copper cable. It can be deduced that the system voltage level and conductor material directly influence cable weight. The optimal combination of 3 kV and an aluminum conductor results in the lowest weight, achieving a substantial 40% reduction in weight.

B. Effect of Battery Pack Number

Commonly, an isolated dc–dc converter is required between the battery side and the HV power system [35]. According to current technical limitations, the volume of MW-level isolated dc–dc converter is large, and the weight is heavy [36]. A lower power converter is easier to manufacture; therefore, if it is difficult to achieve the ideal number of batteries, we need to consider using more battery packs for distributed power supply. This discussion focuses on understanding how the number of batteries directly influences the sizing of cables connecting the batteries to the busbars. The emphasis is on achieving a balance between the challenges of reaching an ideal number of batteries, the demand for power stability, and the weight optimization of the cabling system.

As depicted in Fig. 4(a), an increase in the number of batteries corresponds to a decrease in the output power of each battery. This reduction in output power results in a diminished output current, and subsequently, a smaller cable conductor diameter. Introducing more battery packs leads to a scenario where the actual current flowing through the cable is lower, enabling the adoption of a thinner conductor radius. In this case, however, more number of cables are added. It can be observed that when the actual current passing through the cable is low, there is little difference in weight between copper cables and aluminum cables. Despite aluminum having

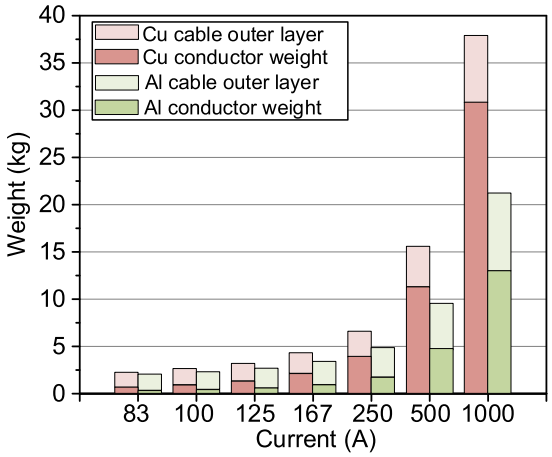

Fig. 5. Weight decomposition of the cable with different rated currents (length: 10 m).

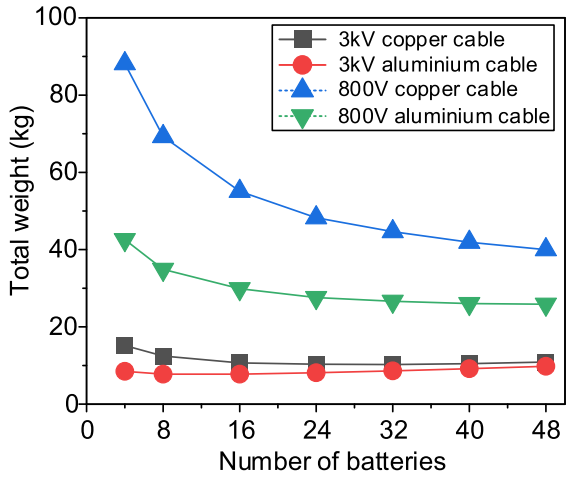

Fig. 6. Influence of the number of battery packs on the total weight of battery side connecting cables (assume one battery pack has a 1-m connection cable).

a lower material density, aluminum cables exhibit a thicker conductor radius under these conditions. From an aircraft weight optimization perspective, aluminum cables can provide a lighter solution. When the weight budget can be met, it is, however, advisable to use copper cables with better overall performance to replace aluminum cables in applications that carry lower currents (<100 A) within the aircraft, as shown in Fig. 4(b). This choice can ensure an optimal balance between weight efficiency and cable performance in electric aircraft applications.

Fig. 5 shows the weight decomposition with different layers. At identical rated voltage and current levels, the weight proportion of copper in copper cables surpasses that of aluminum in aluminum cables. As the current magnitude increases, the weight proportion of the conductor within the cable exhibits a notable ascent. At a current of 1000 A, the copper conductor's weight constitutes over 80% of the total cable weight, whereas the aluminum conductor's weight proportion exceeds 60%. This emphasizes the significant influence of current magnitude on the conductor's contribution to overall cable weight. Conversely, an increased proportion of the outer layer's weight is attributed to the relatively modest change in the thickness requirement of the insulating layer and the jacket. This phenomenon occurs while the conductor thickness decreases under fixed applied voltage conditions. The interplay between the current, conductor material, and the outer layer becomes apparent in shaping the weight distribution across different layers of the cable.

Increasing battery packs affects the whole cabling system weight as well, which is reflected in the length increase of connecting cables between the battery and the HV system. Here, we assume the length of each connection cable from the battery side is 1 m, and battery packs are connected to the system in parallel. The total length of the battery side connecting cable is linear to the battery number. The impact on the total connecting cable weight is shown in Fig. 6. Under 800 V, it can be observed that more parallel battery packs lead to lighter weight. As the number of battery packs increases, the weight-saving advantage, however, is no longer significant, especially when using aluminum cables. Under 3 kV, the trends are different. If aluminum cable is used, the lightest total weight could be achieved with eight battery packs. More battery packs do not lead to a lighter cable. If copper cable is used, the turning point is at 16.

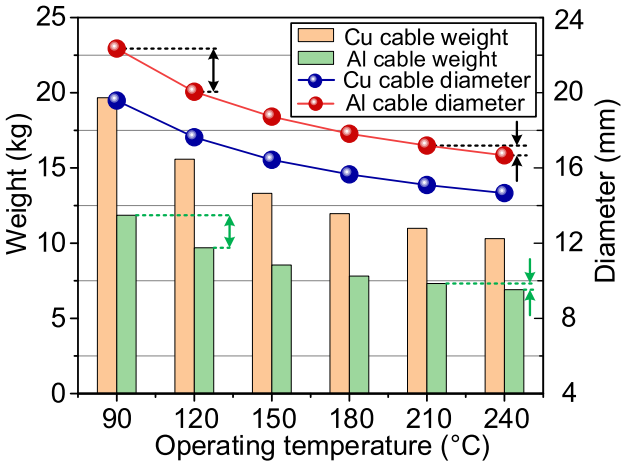

Fig. 7. Weight and dimension of cable with different operating temperatures.

C. Effect of Operating Temperature

Fig. 7 visually represents the impact of various maximum operating temperature choices on the weight and dimensions of the cable. Opting for a higher operating temperature can lead to a reduction in both the weight and diameter of the cable. As the temperature increases, the extent of weight and diameter reduction, however, gradually diminishes. While, in theory, elevating the cable's operating temperature is advantageous for reducing weight in aircraft, it is generally advisable to limit the actual temperature rise under normal operation to less than 40 °C. Despite this, there are no specific standards guiding the design of AEA cables. Choosing 120 °C is a conservative and secure option for cables intended for use in AEA.

There are some factors influencing the cable dynamic temperature rating: operation environment, response time of

protective devices, thermal overload capability, etc. It is noted that generally, the biggest temperature rise occurs when there is a short circuit on the transmission lines. The proposal should integrate protective devices (such as CBs) that respond to contingencies by isolating the faulted sections of the system quickly to prevent cables from being subjected to high currents for prolonged periods. This limits the time cables experience overloads, ensuring their longevity and reducing the risk of failure. When a full discharge occurs, the current flows through the insulation and into the shield. The heat generated by a short circuit current is dependent on the resistance, and the extra heat caused by a short current (Q_{short}) can be expressed as below

$$Q_{\text{short}} = I_{\text{short}}^2 R_{\text{sc}} \Delta t_{\text{CB}} = m_s C' \Delta T \tag{19}$$

where I_{short} is the short current, R_{sc} is the resistance of the short circuit, Δt_{CB} is the response time of the CB, and C' is the specific heat capacity (J/kg·°C^{-1}), which is 385 for copper.

Then, the extra tempertaure rise ΔT casued by short circuit can be deduced by (19). It is noted that $T_{\text{operating}} + \Delta T$ should not exceed 260 °C, which is the tolerance temperature of insulation.

According to the proposal in our research, the allowed response time of switches should be faster than 500 μs if we use 0.12 mm shielding layer.

D. Effect of Power-Sharing Cable

As discussed in Section IV-B, a cable carrying half the power is lighter than 50% of a cable carrying full power. It provides an inspiration that separating the power transmission can reduce the weight of the cabling system. In our architecture design, $n-1$ contingency is considered, and alternative power transmissions are designed. Two cable connections between the battery and HV system are designed in case of one cable or power component failure. If one cable fails or is disconnected, the other will maintain the power supply, necessitating that each connection cable be rated for full power (100%).

The concept of power-sharing transmission with multiple separated cables can, however, decrease the rated power and current for each cable. For example, in the event of a fault in one cable, this cable would be disconnected, leaving three cables available for power transmission. In this scenario, the remaining three cables must share the total power, resulting in each cable being rated at 33% of the total power, as shown in Fig. 8. With four power-sharing cables, the total power capacity becomes 133% of the required power.

Further analysis is conducted to determine if a lighter cabling system could be achieved by increasing the number of separated cables, as shown in Fig. 9. The returning lines are also involved, and aluminum cable is used. It indicates that increasing the number of cables indeed provides significant benefits in terms of weight reduction. The difference is more obvious under 800 V due to a larger current change, while reduced weight gradually decreases with the number of cables. For a 3 kV cable system, increasing the number of cables from two to three results in a weight reduction of 25.8%; however, further increasing the number of cables from three to four

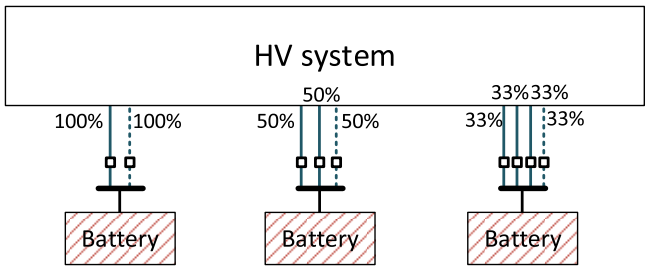

Fig. 8. Concept of power-sharing cable.

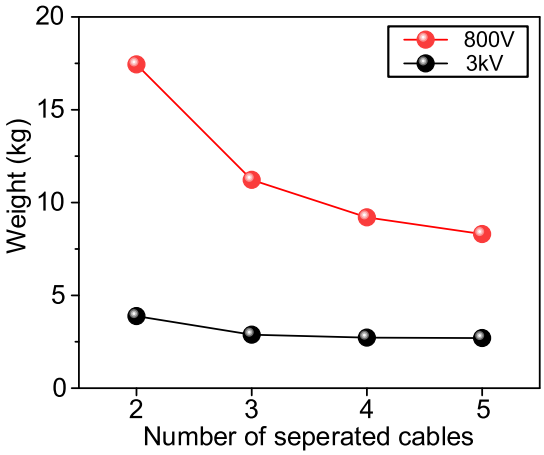

Fig. 9. Relationship between number of power-sharing cables and weight.

yields only a 5% weight reduction, and increasing from four to five provides no significant additional weight reduction.

It can be concluded increasing the number of busbar cables beyond 4 (e.g., from 4 to 5) does not yield additional weight reduction and introduces extra components, necessitating careful consideration of the trade-offs between weight and reliability. According to Fault tree analysis (FTA) [37], the reliability analysis includes the various basic and intermediate events that describe the root causes of the top event with "AND" and "OR." It is mostly used to calculate the probability of such an unwanted event. It can be supposed that the failure of a single power path is a basic event, and the loss of one battery supply is a top event. For the reliability of one power source, several power paths are parallel with the main power supply. Assuming each transmission line has a failure rate of 10^{-4} failures/flight hour, the power source fails if two or more lines fail simultaneously (as the design allows for one line failure while maintaining operation). The failure rates for two, three, and four power-sharing lines are approximately 10^{-8}, 2.9998×10^{-8}, and 5.9992×10^{-8}, respectively.

V. Flight Scenarios and Criteria for Cable Rating Evaluation

The actual cable parameters are mainly driven by the current through the conductor and the applied voltage. Accurate estimation of cable weight is supported by considering the lengths of cables and the actual current under normal conditions, as well as all $n-1$ contingencies [13], [14]. The selection

of cable for electric aircraft is usually dependent on the current under the worst flight scenario. For various power architectures, estimating the current is essential to determine the actual operating status of the circuit under the most adverse flight conditions.

A. Estimation of Cable Length

The dimensions of the aircraft and the proposed architectures are illustrated in Figs. 1 and 2.

In the proposed architecture, eight battery packs are adopted, and they are symmetrically distributed along the wings. A distribution path is designed for cables connecting batteries, busbars, and motors. Two busbars are installed on each wing. Based on the estimated dimensions, the lengths of all cables connecting different buses are calculated and presented in Table IV.

TABLE IV
CABLE LENGTHS IN ARCHITECTURE

From	To	Length (m)	From	To	Length (m)
B1	Bus 1	1	M1	Bus 2	10
B2	Bus 1	5	M2	Bus 2	7
B3	Bus 1	9	M3	Bus 1	7
B4	Bus 1	13	M4	Bus 1	10
B1	Bus 2	10	M3/M4	Bus 2	2
B2	Bus 2	7	Bus 2	Bus 3	10
B3	Bus 2	1	Extender	Bus 1/ Bus 4	23
B4	Bus 2	6	Extender	Bus 2/ Bus 3	16
M1/M2	Bus 1	2			

B. Normal Condition and Single Contingencies

The reliability of the proposed architecture should be assessed under normal conditions and $n-1$ contingencies. Six possible typical scenarios are outlined below. Scenario 1 is the normal flight scenario, and scenarios 2–6 represent abnormal situations. The failure of the busbar would affect multipower paths as there are several cables connecting to it. The failure of the motor means the loss of power load and main power prolusion. The failure of battery packs affects the stable power sources. Both the innermost and outermost faults need to be considered because the failure of power equipment at different locations also affects the power flow of the entire system. The start-up of a reserve energy system and one failure of generators should be considered as well in case of emergency. It is assumed that different single contingencies do not occur simultaneously. These scenarios, used for reliability assessment, should be applied to any proposed architecture.

1) No failure occurs (Solid lines are the active transmission).
2) One busbar fails.
3) One motor fails (including the innermost motor failure and outermost motor failure).
4) One battery fails (including the innermost battery pack failure and outermost motor failure).
5) The battery system is exhausted and reserve energy system starts up (two 6 MW range extenders supply energy through the high voltage system).
6) Reserve energy system fails (one range extender fails, and another range extender is temporarily raised to 7 MW).

The proposed architecture can meet the reliability requirements, ensuring the aircraft's reliable flight in all six scenarios.

C. Evaluation of Rated Current

Under normal operation, the current going through the cables between the motor and the busbar mainly depends on the actual distributed power loads. The continuous power of the motor is 1.5 MW, and the actual current of the interconnections is about 500 A. When one busbar fails, bus 2 or bus 3 failure is the worst case, which means that two battery packs will supply four motors, and the battery side cables will increase the current output. When one motor fails, the power load demand decreases, leading to a reduction in the actual current flowing through the associated connection. In the event of a battery pack failure, where three battery packs supply power to four motors on a single wing, the current at the battery output will increase. This increase in current, however, comes at the expense of a shortened total battery life. For Scenarios 5 and 6, with the reserve energy system activated, the actual current of the interconnections will not exceed that of normal operating conditions. From this observation, it is evident that the connecting cables from motor to busbar can be sized by a rated current of 500 A. For the cables from the battery side, in the case of a solid line connection, it is, however, necessary to increase the rated current to 1000 A to accommodate potential emergencies.

According to Table IV, the length for each power cable is provided. For the normal operation system, the maximum length of a single cable is 13 m, and the voltage drop of $<0.02\%$. The maximum connecting length from the battery to the motor is 20 m, and the total voltage drop is below 0.04%. The value is allowed for the whole electrical system operation, and efficient power delivery is ensured.

VI. WEIGHT EVALUATION

Following the methods for calculating cable size and weight, as well as the criteria for selecting cable-rated current, Table V provides a weight comparison of the high-voltage cable system at 800 V and 3 kV. In this comparison, only the weight of the cable and busbar is taken into account. The chosen busbar is the conventional metal type. The busbar is rated at 2000 A under 3 kV to meet the current requirements. In the event of Scenario 2, a single busbar supplies four motors simultaneously, and the potential maximum current in this case could reach 2000 A. The mass of each busbar strip is about 10 kg. When the voltage level turns to 800 V, a larger current leads to a heavier busbar, which can reach about 43 kg. [38].

It can be seen that increasing the voltage from 800 V to 3 kV has a significant impact on the weight of the cable system. Although the current is 3.75 times higher, the system weight is 5.69 times greater for copper cables and 4.82 times greater for aluminum cables. The use of 3 kV and aluminum cables can save a significant amount of weight, and in this

TABLE V
WEIGHT COMPARISON BETWEEN 3 kV SYSTEM AND 800 V SYSTEM (kg)

		3kV	800 V
1	Busbar [34]	4*10.0 =40.0	4*43.0=172.0
2	Connection cable (battery—busbar)	Cu:322.4 Al: 201.8	Cu: 1799.2 Al: 906.9
3	Connection cable (motor—busbar)	Cu: 260.4 Al: 164.0	Cu: 1453.2 Al: 732.5
4	Range extender cable	Cu: 383.2 Al: 196.8	Cu: 2271.6 Al: 1060.4
5	Connection cable between two busbars	Cu: 174.6 Al: 94.3	Cu: 1018.8 Al: 484.6
Total weight of cabling system		Cu: 1180.6 Al: 696.9	Cu: 6714.8 Al: 3356.4

case, the cabling system weight would be below 700 kg. This is an optimistic result for reducing the weight of the aircraft. Because of the highly rated power of the range extender, these cables account for about one-third of the system's total weight. Optimizing the layout of the range extender could potentially further reduce the weight of the cable system.

VII. CONCLUSION

In this article, a electric power system architecture with high realility was proposed for a 90 seater AEA. The cable sizing method for high voltage aerospace applications was introduced and the effect of voltage level, battery number, current, and operation temperature was studied. This article estimates the weight of the cable system for large electric aircraft based on practical case calculations. The main findings are concluded as follows.

1) The advantages of increasing voltage are particularly noticeable in cable weight reduction, especially for copper cables. The use of an aluminum conductor, PTFE insulator material, and a voltage level of 3 kV proves to be a preferable selection for current AEA medium and high voltage cables.
2) At the rated voltage of 3 kV, when the rating current is less than 100 A, the advantage of aluminum cables in weight reduction may not be apparent. 120 °C operating temperature is a conservative and secure option for cables intended for use in AEA.
3) In the case of a 3 kV system, more battery packs do not lead to a lighter cable. If aluminum cable is used, the lightest total weight could be achieved with eight battery packs.
4) Separating the power transmission can reduce the weight of the cabling system. The specific architecture design, however, must also consider the reduction in system reliability caused by an increase in the number of power components.
5) For the proposed architecture, the rating of various interconnection cables is driven directly by the actual power supply proportions. For a 3 kV aluminum cable system, its weight budget could be controlled below 700 kg.

REFERENCES

[1] (May 2021). *Net-Zero Carbon Emissions by 2050*. [Online]. Available: https://www.iea.org/reports/net-zero-by-2050

[2] B. Sarlioglu and C. T. Morris, "More electric aircraft: Review, challenges, and opportunities for commercial transport aircraft," *IEEE Trans. Transport. Electrific.*, vol. 1, no. 1, pp. 54–64, Jun. 2015, doi: 10.1109/TTE.2015.2426499.

[3] (May 2021). *Recognizing Growing Urgency, Global Leaders Call for Concrete Commitments for Clean, Affordable Energy for All by 2030 and Net-Zero Emissions by 2050*. [Online]. Available: https://www.un.org/en/desa/clean-affordable-energy

[4] IEA, Paris, France. (2021). *An Energy Sector Roadmap to Carbon Neutrality in China*. [Online]. Available: https://www.iea.org/reports/an-energy-sector-roadmap-to-carbon-neutrality-in-china

[5] A. Barzkar and M. Ghassemi, "Electric power systems in more and all electric aircraft: A review," *IEEE Access*, vol. 8, pp. 169314–169332, 2020, doi: 10.1109/ACCESS.2020.3024168.

[6] Airbus. *A380: Unique Passenger Experience*. Accessed: Oct. 15, 2019. [Online]. Available: https://www.airbus.com/aircraft/passengeraircraft/a380.html

[7] Boeing. *Boeing 787, Dreamliner*. [Online]. Available: http://www.boeing.com/commercial/787/

[8] H. Schefer, L. Fauth, T. H. Kopp, R. Mallwitz, J. Friebe, and M. Kurrat, "Discussion on electric power supply systems for all electric aircraft," *IEEE Access*, vol. 8, pp. 84188–84216, 2020, doi: 10.1109/ACCESS.2020.2991804.

[9] NASA Glenn Res. Center. (2021). *Turboelectric*. Accessed: Nov. 1, 2021. [Online]. Available: https://www1.grc.nasa.gov/aeronautics/eap/airplane-concepts/turboelectric

[10] R. E. Wolleswinkel, R. de Vries, M. Hoogreef, and R. Vos, "A new perspective on battery-electric aviation, Part I: Reassessment of achievable range," in *Proc. AIAA SCITECH Forum*, Orlando, FL, USA, Jan. 2024, p. 1489, doi: 10.2514/6.2024-1489.

[11] R. de Vries, R. E. Wolleswinkel, M. Hoogreef, and R. Vos, "A new perspective on battery-electric aviation, Part II: Conceptual design of a 90-seater," in *Proc. AIAA SCITECH Forum*, Orlando, FL, USA, Jan. 2024, p. 1490, doi: 10.2514/6.2024-1490.

[12] A. Barzkar and M. Ghassemi, "Components of electrical power systems in more and all-electric aircraft: A review," *IEEE Trans. Transport. Electrific.*, vol. 8, no. 4, pp. 4037–4053, Dec. 2022, doi: 10.1109/TTE.2022.3174362.

[13] M. Ghassemi, A. Barzkar, and M. Saghafi, "All-electric NASA N3-X aircraft electric power systems," *IEEE Trans. Transport. Electrific.*, vol. 8, no. 4, pp. 4091–4104, Dec. 2022, doi: 10.1109/TTE.2022.3158186.

[14] M. J. Armstrong et al., "Architecture, voltage and components for a turboelectric distributed propulsion electric grid," Nat. Aeronaut. Space Admin., Hampton, VA, USA, Tech. NASA/CR-2015-218440, 2015.

[15] J. Haglage, T. Dever, R. Jansen, and M. Lewis, "Electrical system trade study for SUSAN Electrofan concept vehicle," in *Proc. AIAA SCITECH Forum*, San Diego, CA, USA, Jan. 2022, p. 2183.

[16] A. Azizi and M. Ghassemi, "Design of high power density MVdc cables for wide body all electric aircraft," *IEEE Trans. Dielectr. Electr. Insul.*, vol. 30, no. 5, pp. 2315–2324, Oct. 2023, doi: 10.1109/TDEI.2023.3285849.

[17] *Standard Practice for Design, Alteration, and Certification of Aircraft Electrical Wiring Systems*, ASTM Standard F2639-18, 2018.

[18] *Wire, Electrical, Fluoropolymer-Insulated, Copper or Copper Alloy*, SAE Standard AS22759D, 2018.

[19] *Power Cables With Extruded Insulation and Their Accessories for Rated Voltages From 1 KV Up to 30 KV*, IEC Standard 60502-2, Int. Electrotechnical Commission, Geneva, Switzerland, 2005.

[20] G. J. Anders, "Review of power cable standard rating methods," in *Rating of Electric Power Cables in Unfavorable Thermal Environment*. Hoboken, NJ, USA: Wiley, 2005, pp. 1–75, doi: 10.1109/9780471718741.ch1.

[21] T. C. Cano et al., "Future of electrical aircraft energy power systems: An architecture review," *IEEE Trans. Transport. Electrific.*, vol. 7, no. 3, pp. 1915–1929, Sep. 2021, doi: 10.1109/TTE.2021.3052106.

[22] E. Aretskin-Hariton, M. Bell, S. Schnulo, and J. S. Gray, "Power cable mass estimation for electric aircraft propulsion," in *Proc. AIAA Aviation Forum*, 2021, p. 3021, doi: 10.2514/6.2021-3021.

[23] C. Wijnveen, "Design of propulsion system for 9 PAX electric aircraft," M.S. thesis, Dept. Elect. Sustain. Energy, Delft Univ. Technol., Delf, The Netherlands, 2022.

[24] T. L. Bergman et al., *Fundamentals of Heat and Mass Transfer*, 7th ed., Hoboken, NJ, USA: Wiley, 2011.

[25] F. P. Incropera et al., *Fundamentals of Heat and Mass Transfer*, 6th ed., Hoboken, NJ, USA: Wiley, 2007.

[26] G. F. Hewitt, G. L. Shires, and T. R. Bott, *Process Heat Transfer*. Boca Raton, FL, USA: CRC Press, 1994.

[27] M. A. Boles and Y. A. Çengel, *Thermodynamics: An Engineering Approach*. New York, NY, USA: McGraw-Hill, 2019.

[28] *Wires & Cables for Aerospace Applications*. Accessed: 2017. [Online]. Available: https://www.prysmiangroup.com/sites/default/files/atoms/files/Catalogue%20AEROSPACE.pdf

[29] *PTFE and PFA Similarities and Differences*. Accessed: May 2017. [Online]. Available: https://www.emerson.com/documents/automation/white-paper-ptfe-pfa-similarities-differences-rosemount-en-585104.pdf

[30] H. Teng, "Overview of the development of the fluoropolymer industry," *Appl. Sci.*, vol. 2, no. 2, pp. 496–512, May 2012.

[31] F. C. Cheng, "Insulation thickness determination of polymeric power cables," *IEEE Trans. Dielectr. Electr. Insul.*, vol. 1, no. 4, pp. 624–629, Aug. 1994, doi: 10.1109/94.311705.

[32] P. K. Cheo, R. Luther, and J. W. Porter, "Detection of voids and contaminants in polyethylene insulated cable utilizing a fir laser beam," *IEEE Trans. Power App. Syst.*, vol. PAS-102, no. 3, pp. 521–526, Mar. 1983, doi: 10.1109/TPAS.1983.317971.

[33] Mide Technol. Corp., Woburn, MA, USA. *Air Pressure at Altitude Calculator*. [Online]. Available: https://www.mide.com/air-pressure-at-altitude-calculator

[34] T. W. Dakin et al., "Breakdown of gases in uniform fields Paschen curves for nitrogen, air and sulfur hexafluoride," *Electra*, vol. 32, pp. 61–82, 1974. [Online]. Available: https://www.e-cigre.org/publications/detail/elt-032-4-breakdown-of-gases-in-uniform-fields-paschen-curves-for-nitrogen-air-and-hexafluoride.html

[35] B. Patnaik, S. Kumar, and S. Gawre, "Recent advances in converters and storage technologies for more electric aircrafts: A review," *IEEE J. Miniaturization Air Space Syst.*, vol. 3, no. 3, pp. 78–87, Sep. 2022, doi: 10.1109/JMASS.2022.3200715.

[36] N. Keshmiri, M. I. Hassan, R. Rodriguez, and A. Emadi, "Comparison of isolated bidirectional DC/DC converters using WBG devices for more electric aircraft," *IEEE Open J. Ind. Electron. Soc.*, vol. 2, pp. 184–198, 2021, doi: 10.1109/OJIES.2021.3058196.

[37] X. Shi and A. M. Bazzi, "Fault tree reliability analysis of a microgrid using Monte Carlo simulations," in *Proc. IEEE Power Energy Conf. Illinois (PECI)*, Champaign, IL, USA, Feb. 2015, pp. 1–5, doi: 10.1109/PECI.2015.7064928.

[38] *Copper Busbar Rating*. [Online]. Available: https://www.australwright.com.au/technical-data/advice/copper-busbar-rating/